

Design and demonstration of an adiabatic-quantum-flux-parametron field-programmable gate array using Josephson-CMOS hybrid memories

Yukihiro Okuma, Naoki Takeuchi, Yuki Yamanashi, *Member, IEEE* and Nobuyuki Yoshikawa, *Senior Member, IEEE*

Abstract—Adiabatic quantum-flux-parametron (AQFP) logic is a promising technology for future energy-efficient high-performance information processing systems. Its static power is zero because of ac flux bias, and its dynamic power is considerably reduced thanks to the adiabatic switching of the junctions. The lack of high-density memories in the AQFP logic, however, makes it challenging to realize large-scale information processing systems with the use of pure AQFP circuits. We have been developing a Josephson-CMOS hybrid memory to overcome the memory bottleneck in AQFP digital systems. By utilizing the high sensitivity of the AQFP gate, the output current from CMOS memories can be significantly decreased resulting in the reduction of the power consumption. In this study, we designed and fabricated a low-power area-efficient AQFP-CMOS hybrid field-programmable gate array (FPGA), where a CMOS memory is utilized as a rewritable read-only memory to control the AQFP circuits. The AQFP circuit for the AQFP-CMOS hybrid FPGA is composed of logic blocks, switch blocks and connection blocks, which are clocked by four-phase excitation currents. The AQFP-CMOS hybrid FPGA is fabricated by using the AIST 10 kA/cm² Nb high-speed standard process and the Rohm 0.18 μ m CMOS process. The area and power consumption of the two-by-two AQFP logic-cell system are estimated to be about 6.56 mm² and 12.4 nW at 5 GHz operations, respectively. The power consumption of the CMOS memory was estimated to be 1.02 μ W assuming the CMOS source voltage of 3 mV. We demonstrated the operation of the AQFP-CMOS hybrid FPGA at low speed by combining the AQFP logic and the CMOS memory.

Index Terms—Superconducting integrated circuits, Hybrid memory, Adiabatic quantum-flux-parametron, adiabatic logic, Field programmable gate arrays, CMOS.

Y. Okuma is with Department of Electrical and Computer Engineering, Yokohama National University, 79-5 Tokiwadai, Hodogaya, Yokohama 240-8501, Japan (e-mail: okuma-yukihiro-gz@ynu.jp).

N. Takeuchi is with the Institute of Advanced Sciences, Yokohama National University, 79-5 Tokiwadai, Hodogaya, Yokohama 240-8501, Japan; PRESTO, Japan Science and Technology Agency, 4-1-8 Honcho, Kawaguchi, Saitama 332-0012, Japan (e-mail: takeuchi-naoki-kx@ynu.jp).

Y. Yamanashi and N. Yoshikawa are with the Institute of Advanced Sciences, Yokohama National University, 79-5 Tokiwadai, Hodogaya, Yokohama 240-8501, Japan; Department of Electrical and Computer Engineering, Yokohama National University, 79-5 Tokiwadai, Hodogaya, Yokohama 240-8501, Japan (e-mail: yamanashi-yuki-kr@ynu.ac.jp, nyoshi@ynu.ac.jp).

I. INTRODUCTION

THE performance of semiconductor integrated circuits has been continuously and rapidly improved due to advances in microfabrication technology. However, in recent years, microfabrication technology is considered to be approaching limitation [1]. Low-power superconductor logic families are attractive as a fundamental technology for future high-performance information processing systems. Various superconductor logic families such as rapid single-flux-quantum (RSFQ) logic [2] have been extensively studied [3] - [5]. Adiabatic quantum-flux-parametron (AQFP) logic [6] is an energy-efficient superconductor logic based on the quantum-flux-parametron (QFP) [7], [8]. The static power of AQFP logic is zero because of ac flux biasing. In addition, the dynamic power of AQFP logic is considerably reduced thanks to adiabatic switching of the junctions [9], [10]. As a result, the bit energy of AQFP logic is about six orders of magnitude lower than that of semiconductor logic [11]. Recently average energy dissipation of 1.5 zJ per junction was demonstrated in an 8-bit carry-lookahead adder at 5 GHz [12]. The lack of high-density memories in the AQFP logic, however, makes it challenging to realize large-scale computing systems using pure AQFP circuits. One way to overcome the memory bottleneck is the hybridization of superconducting logic with CMOS logic [13] - [15]. Recently we demonstrated the fully functional operation of 64-kb Josephson-CMOS hybrid memories [16]. In this system, small signals from RSFQ circuits are amplified by using Josephson latching drivers and CMOS amplifiers; then the signals are provided to a CMOS memory composed of 8-transistor static memory cells. The output signals from CMOS memory cells are detected by RSFQ-based current sensors. Because of the high current sensitivity of the RSFQ current sensor, high-speed memory access can be expected. One drawback in this system is relatively high power consumption necessary to amplify the small signal from the RSFQ circuits and to decode the address data at high speed. It was estimated that about 93% of power is consumed at the amplifiers and decoders in the hybrid memory [16]. These high power consumption can be prevented by using a hybrid memory as a rewritable read-only memory (ROM), where the write operation happens relatively infrequently.

Moreover, CMOS bias voltage for reading the memory data can be reduced independently from the entire CMOS bias voltage to decrease the power consumption of the memory. Considering the high current sensitivity of the AQFP gates of a few μA levels, the power consumption of the hybrid memory can be considerably decreased.

A field-programmable gate array (FPGA) [17] is a kind of programmable logic devices (PLD), which is integrated circuits realizing arbitrary logic functions. Though the FPGA was traditionally used to test the functionality of a prototype system, it is recently used even as an accelerator in the high-performance computing system due to its reconfigurability and large-scale hardware parallelism. High-performance FPGAs composed of more than 1 M logic cells have been manufactured by using the 16 nm Fin FET technology [18]. In the high-performance FPGA, the performance per watt is one of the essential figures of merits. However, a large portion of the power of the latest CMOS FPGAs is consumed by the leakage currents of CMOS devices, which limits the device performance. Thus superconducting integration circuits are attractive to realize FPGAs due to their energy-efficient operation. The first superconducting FPGA using RSFQ circuits was proposed in [19], in which an FPGA with two-by-two logic cells was designed, and its hardware cost was estimated. Recently an RSFQ-based FPGA using magnetic Josephson junction memories was proposed for implementation

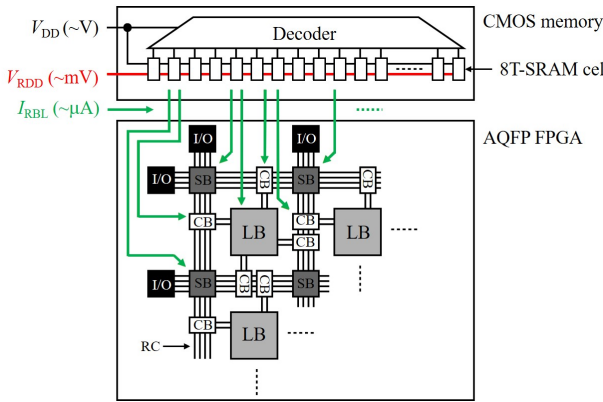


Fig. 1 Conceptual diagram of an AQFP-CMOS hybrid FPGA using a Josephson-CMOS hybrid memory.

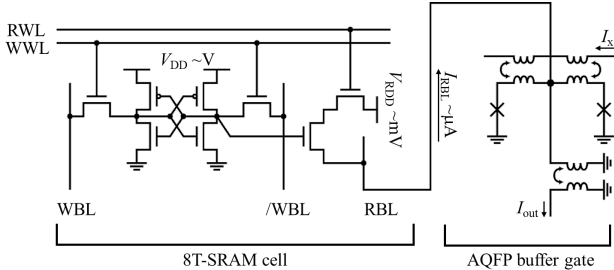


Fig. 2 Circuit diagram of an 8-T SRAM cell and an AQFP buffer gate to detect the readout signal from the 8-T SRAM cell. RWL and WWL represent a read word line and a write word line, respectively. WBL and /WBL are a write bit line and its complement. RBL is a readout bit line. The supply voltage V_{DD} is applied to the entire CMOS gates except the supply voltage V_{RDD} applied to readout transistors. I_{RBL} denotes the output current from an 8T-SRAM cell. I_x and I_{out} are an excitation current and an output current of the AQFP buffer gate, respectively.

of area-efficient switches [20]. Nevertheless, both of these activities are theoretical researches, and no actual system is demonstrated up to now.

In this study, we propose an AQFP-CMOS hybrid FPGA by using a CMOS memory as a rewritable ROM. The power consumption of the CMOS memory can be significantly reduced by decreasing the supply voltage for a CMOS memory. We designed and implemented an AQFP-CMOS hybrid FPGA with two-by-two logic cells, and estimated their hardware cost. Their functionality was examined at low speed.

II. AQFP-CMOS HYBRID FPGA

Fig.1 shows a conceptual diagram of an AQFP-CMOS hybrid FPGA using a CMOS memory. The system is composed of an AQFP FPGA circuit and a CMOS memory. The AQFP FPGA circuit is a two-dimensional array of logic cells composed of logic blocks (LBs), switch blocks (SBs) and connection blocks (CBs). I/O blocks are connected to the peripheral of the logic cell array. The CMOS memory defines the function of the AQFP FPGA circuit by applying μA level currents to each AQFP gate. The CMOS memory is composed of a CMOS decoder and 8-transistor (8-T) SRAM cells. The decoder and memory cells are driven by typical CMOS supply voltage V_{DD} of volt levels, while the readout transistors are driven by much lower supply voltage V_{RDD} of mV levels. The data of the CMOS memory are directly written from the room temperature electronics through the CMOS decoder. The detailed design of the CMOS decoder and 8-T SRAM cells are described in [16].

Fig. 2 shows a circuit diagram of an 8-T SRAM cell and an AQFP buffer gate to detect the current from the 8-T SRAM cell. By separating the supply voltage V_{RDD} of the readout transistors from the supply voltage V_{DD} of the entire CMOS circuits, the readout current, and hence the power consumption can be considerably reduced. The dependence of the measured output current I_{RBL} of the 8T-SRAM cell on the supply voltage V_{RDD} of readout transistors is shown in Fig. 3. We used Rohm $0.18 \mu\text{m}$ CMOS devices whose typical supply voltage is 1.8 V. The width of the readout transistor is $5 \mu\text{m}$. Since the current

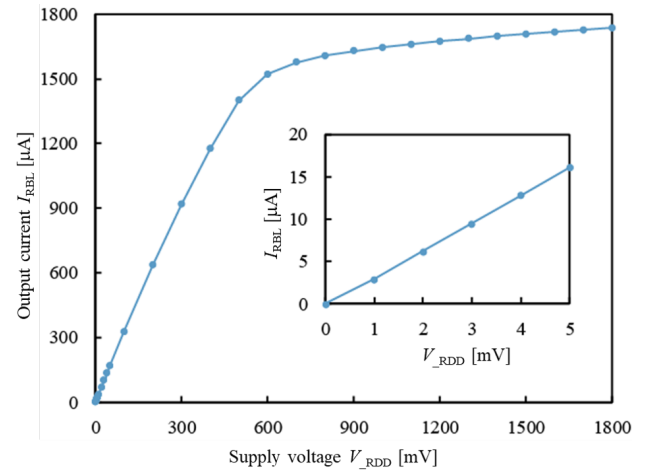


Fig. 3 Dependence of the output current I_{RBL} from the 8T-SRAM cell on the supply voltage V_{RDD} to readout transistors. The inset shows an enlarged graph near the origin.

sensitivity of AQFP buffer gates is a few μA level, we can evaluate V_{RDD} necessary for reading the memory data. When we assume the output current of the memory cells is $10 \mu\text{A}$, we can choose V_{RDD} to be 3 mV, and the power consumption of the memory is estimated to be 30 nW/bit.

III. DESIGN OF AN AQFP FPGA CIRCUIT

Fig. 4 shows block diagrams of the AQFP FPGA circuit designed in this study. The AQFP FPGA circuit is mainly composed of four circuit blocks: a logic block (LB), a switch block (SB), an input connection block (iCB), and an output connection block (oCB). LB is a programmable logic gate with two inputs and one output, whose function can be defined by a 4-bit look-up table (LUT). SB is a programmable switch gate with four inputs and four outputs, where output signals from the bottom and left nodes are selected among either of the top or right nodes. iCB is a programmable switch gate with two inputs and four outputs, where output signals of the bottom nodes are selected among either of the right nodes. oCB is a programmable switch gate with three input and two outputs, where the input signal from the top nodes is switched to output nodes. In order to reduce the hardware cost, the direction of the signal flow in the routing channel (RC) is restricted as shown in Fig. 4.

Each AQFP circuit block was designed by using the AQFP logic cell library for the AIST 10 kA/cm² Nb high-speed standard process [21] based on the minimalist design approach [22]. Fig. 5 shows a circuit diagram of LB, which consists of a 4-to-1 multiplexer (MUX) and a feedback-type delay latch

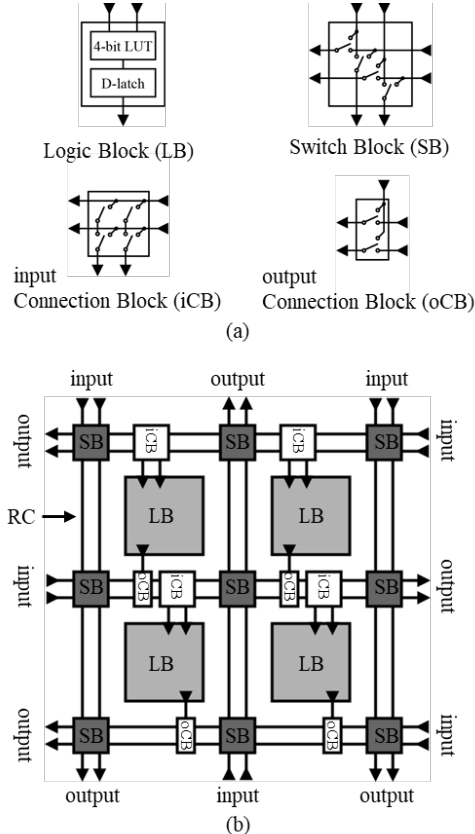


Fig. 4 Block diagram of the AQFP FPGA circuit. (a) Basic blocks. (b) A two-by-two logic-cell system.

(D-latch) [23]. Control data for a 4-to-1 MUX are supplied from a CMOS memory, which stores the LUT data for the LB. The circuit is driven by four-phase excitation clocks I_{x1} through I_{x4} so that the input data is output at the next two clock cycle. The circuit area and the junction number are estimated to be $345 \times 520 \mu\text{m}^2$ and 86, respectively. Fig. 6 shows circuit diagrams of SB, iCB and oCB. Their main circuit element is a 2-to-1 multiplexer (2M), which selects one of two input signals depending on a control signal from a CMOS memory. All the circuits are driven by four-phase excitation clocks so that the input data is output at the next clock cycle. The circuit area of SB, iCB and oCB are $315 \times 600 \mu\text{m}^2$, $315 \times 350 \mu\text{m}^2$, and $315 \times 600 \mu\text{m}^2$, respectively. Their junction numbers are 96, 60 and 50, respectively.

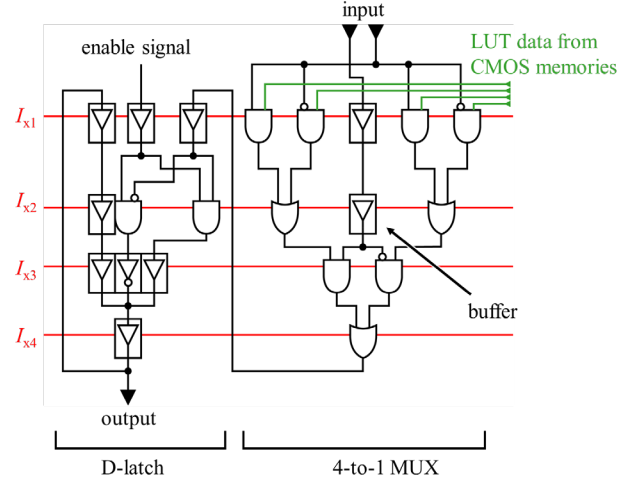


Fig. 5 Circuit diagram of a logic block (LB). I_{x1} , I_{x2} , I_{x3} and I_{x4} denote 4-phase excitation currents.

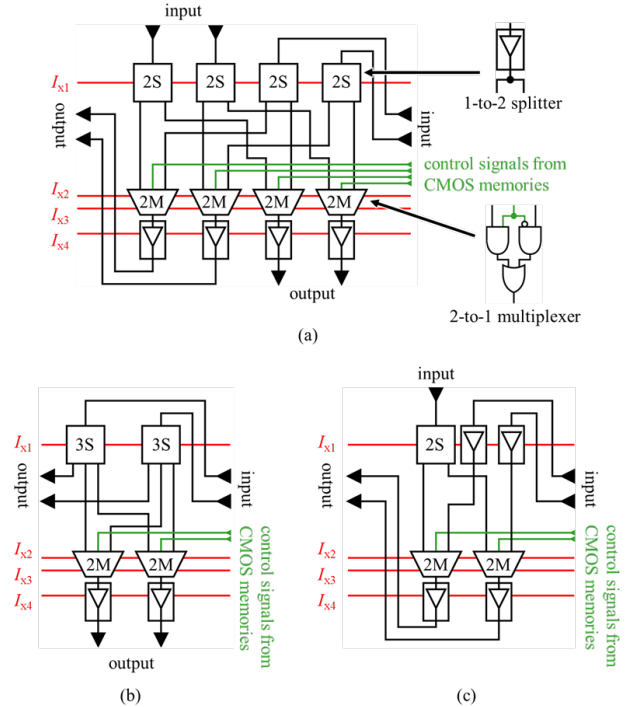


Fig. 6 Circuit diagrams of switching elements. (a) Switch block (SB). (b) Input connection block (iCB). (c) Output connection block (oCB). I_{x1} , I_{x2} , I_{x3} and I_{x4} are 4-phase excitation currents.

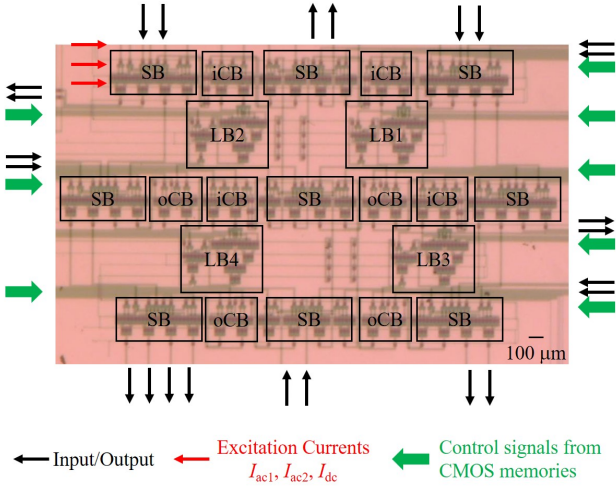


Fig. 7 Photomicrograph of the AQFP FPGA circuit composed of two-by-two logic cells.

TABLE I

Breakdown of the junction number and the number of CMOS memory cells on the AQFP FPGA circuit with two-by-two logic cells.

	Number of blocks	Number of Josephson junctions	Number of CMOS memory cells
LB	4	344	16
SB	9	864	36
iCB	4	240	8
oCB	4	200	8
Others	-	32	-
Total	-	1680	68

Fig. 7 shows a photomicrograph of a two-by-two AQFP FPGA circuit fabricated by using the AIST 10 kA/cm² Nb high-speed standard process. The system is composed of four LBs, nine SBs, four iCBs and four oCBs. The total circuit area is estimated to be 1960×3350 μm². The junction number and the number of CMOS memory cells are listed in TABLE I. Four-phase excitation currents I_{x1} through I_{x4} are generated by the combination of two ac currents I_{ac1} and I_{ac2} , and one dc bias current I_{dc} , whose designed amplitudes are 782 μA, 782 μA and 1070 μA, respectively. The power consumption of the AQFP circuit is estimated to be 12.4 nW at 5 GHz, whereas that of the CMOS memories is 1.02 μW assuming $V_{RDD} = 3$ mV.”

IV. MEASUREMENT OF AN AQFP-CMOS HYBRID FPGA

Fig. 8 shows a photograph of a two-by-two AQFP-CMOS hybrid FPGA using a CMOS memory. In this study, we use a CMOS memory for controlling four AQFP LUTs. The total number of control lines from the CMOS memory is 16 because each LUT has four control lines. The CMOS memory is composed of a 4-to-16 decoder and sixteen 8T-SRAM cells, which was fabricated by using the Rhom 0.18 μm CMOS process. A Josephson chip and a CMOS chip are connected by Al wire bonding.

Fig.9 is an example of the circuit configuration of the AQFP-CMOS hybrid FPGA in a functional test. Because of the malfunction of the bottom two logic blocks, we tested the function of the top two logic blocks. By applying the control signals to the routing channel from room-temperature

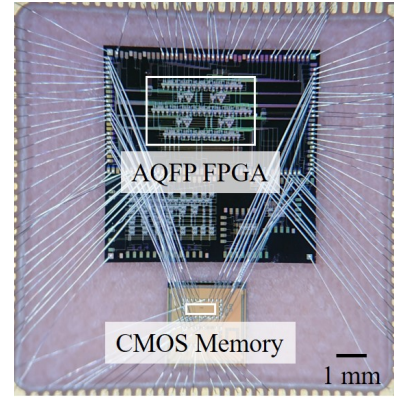


Fig. 8 Photograph of an AQFP-CMOS hybrid FPGA.

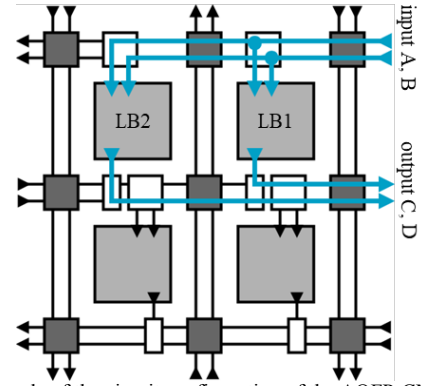


Fig. 9 Example of the circuit configuration of the AQFP-CMOS hybrid FPGA in a functional test.

electronics, we defined the circuit configuration as shown in Fig. 9.

Fig. 10 shows an example of measured waveforms. In the first test sequence, at first, we loaded the data “0001” and “0110” to the CMOS memory by varying the address successively to set the function of LB1 and LB2 to be AND and XOR. Then V_{RWL} was enabled to send the data to the AQFP circuits. In this test, V_{RDD} was set to 15 mV to obtain large memory output current. After that, the input signals I_{inA} and I_{inB} are applied, and output signals V_{outC} and V_{outD} were measured. One can see that AND and XOR functions are properly obtained in LB1 and LB2. It should be noted that the output data from LB1 appear earlier than those from LB2 by five cycles. This is because the length of the routing channel is different as shown in Fig. 9. In the second test sequence, the data “1110” and “0111” are loaded to the CMOS memory to set the function of LB1 and LB2 to be NAND and OR, respectively. One can see that the correct functions were obtained in V_{outC} and V_{outD} . The measured operation margins for the excitation currents I_{ac1} , I_{ac2} and I_{dc} are ±39% (439 - 990 μA), ±38% (439 - 969 μA) and ±24% (745 - 1224 μA), respectively.

V. DISCUSSIONS

The junction number, circuit area, memory cell number, power consumption of the AQFP-CMOS hybrid FPGAs with two-by-two and 32-by-32 logic cells are listed in TABLE II. Notice that these parameters proportionally increase with the increase of the number of logic cells because of scaling of the

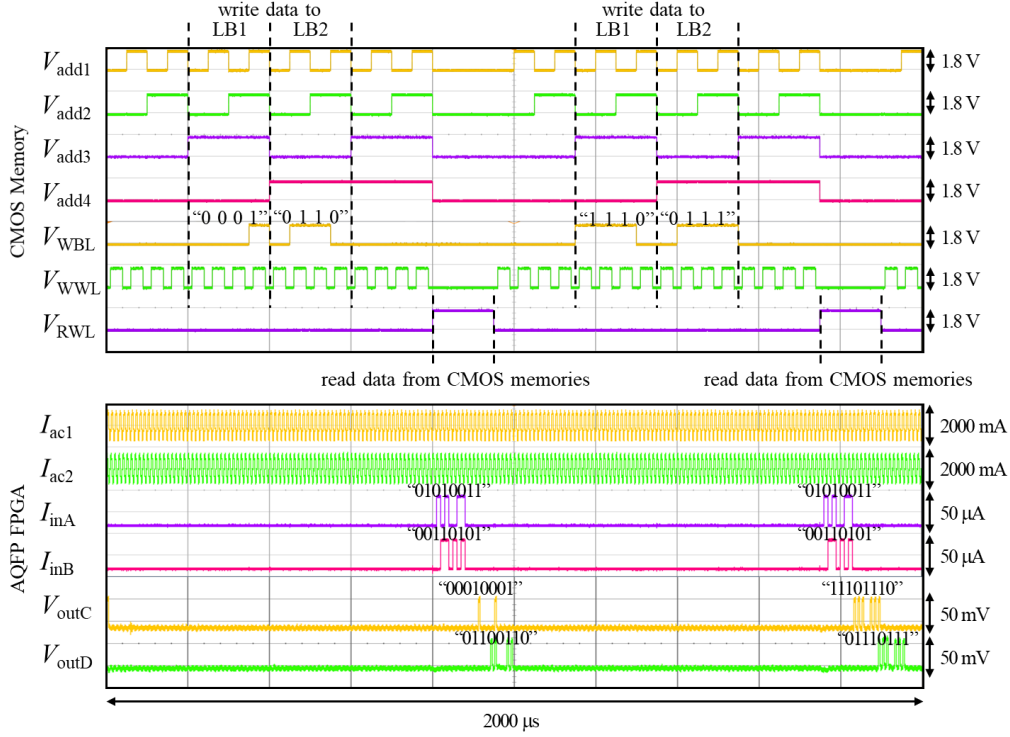


Fig. 10 Example of measured waveforms of the AQFP-CMOS hybrid FPGA. V_{add1} , V_{add2} , V_{add3} and V_{add4} are address signals for a 4-to-16 decoder. V_{WBL} , V_{WWL} and V_{RWL} are input signals for the 8T-SRAM cells. I_{ac1} and I_{ac2} are excitation currents for the AQFP circuit. I_{inA} and I_{inB} are input current to the AQFP circuit, and V_{outC} and V_{outD} are output voltages from the AQFP circuit. The supply voltage to the CMOS memory V_{DD} is 1.8 V. **The output data V_{outC} and V_{outD} appear after 8 and 13 cycles, respectively, from the input of the data I_{inA} and I_{inB} . Notice that one cycle of the additional delay exists due to four stages of output buffers, which are used to amplify the output signals.**

system. In the estimation of the power consumption of the CMOS memory, we assumed V_{RDD} to be 3 mV. The circuit area will be further reduced by revising the sparse layout in the current design. Furthermore, the use of a multi-layer Josephson integrated process [24] will reduce the area of the circuits significantly. Our estimation indicated that the cell size could be reduced to about 40% of the current design. The double active-layered process, where Josephson junctions are fabricated in the different metal layers, also helps to increase the circuit density [25].

Though we use wire bonding to connect AQFP and CMOS chips in the current demonstration, we plan to use flip-chip bonding with the pad pitch of about 150 μm in the next step, which increases the number of AQFP-CMOS connections to several hundred levels. However, more dense connections by using a Josephson/CMOS monolithic fabrication process have to be developed for realizing larger systems.

The estimation of the power consumption in TABLE II shows that about a hundred time larger power is consumed in CMOS memories than AQFP FPGA circuits. It should be noted that the power consumption of the CMOS memory can be further reduced by decreasing the on-state resistance of the MOS device. This can be simply obtained by increasing the device width or by using a newer CMOS fabrication process. In this case, the possible lowest on-state resistance is limited by the thermal noise current given by $I_N = (4k_B T \Delta f / R)^{1/2}$, where k_B is the Boltzmann constant, T is operating temperature, Δf is the bandwidth, and R is the on-state resistance of the MOS device. For $R = 1 \Omega$, $\Delta f = 5 \text{ GHz}$, and $T = 4.2 \text{ K}$, we can estimate the thermal noise current to be $I_N = 1.1 \mu\text{A}$, which is still smaller

TABLE II
Junction number, circuit area, memory cell number, power consumption of AQFP-CMOS hybrid FPGAs with two-by-two and eight-by-eight logic cells.

	2×2 logic cell system	32×32 logic cell system
Junction number of AQFP FPGA circuits	1680	313220
Area of AQFP FPGA circuits [μm^2]	1960×3350	36085×44600
Number of CMOS memory cells	68	12548
Power consumption of AQFP FPGA circuits [nW]	12.4	2348
Power consumption of CMOS memories [μW]	1.02	188

than the output signal current ($\sim 10 \mu\text{A}$) from the MOS device. For $R = 1 \Omega$, the power consumption of the CMOS memory is estimated to be about 0.1 nW/bit, which makes the values in TABLE II 100-fold smaller.

As stated in the previous section, the latency of each wiring block, SB, iCB, and oCB is one cycle, whereas that of the logic block, LB is two cycles. Therefore the latency for wiring is at least two cycles between neighboring logic blocks, and it will increase proportionally with an increase of the distance between logic blocks. The disadvantage of the large interconnection latency of the AQFP FPGA as compared to conventional AQFP circuits with a maximum interconnection length of about 1 mm must be compensated by the system's reconfigurability in practical applications.

VI. CONCLUSION

We proposed a low-power area-efficient AQFP-CMOS hybrid FPGA, where a CMOS memory was used as a rewritable read-only memory. The energy consumption of the CMOS memory was considerably reduced by decreasing the supply voltage to the MOS device for reading out. The proposed AQFP FPGA circuit is composed of four circuit blocks: logic blocks, switch blocks, input connection blocks, and output connection blocks, to which control signals are supplied from the CMOS memory cells. We designed and implemented an AQFP-CMOS hybrid FPGA with 2×2 logic cells by using the AIST 10 kA/cm² Nb high-speed standard process and the Rohm 0.18 μm CMOS process. It was shown that the power consumption of the AQFP FPGA circuit is 12.4 nW at 5 GHz, whereas the power consumption of the CMOS memory was estimated to be 1.02 μW assuming the CMOS source voltage of 3 mV. We confirmed the correct operation the AQFP-CMOS hybrid FPGA at low speed.

ACKNOWLEDGMENT

This work was supported by JSPS KAKENHI Grant Number 26220904. This work was supported in part by VLSI and Education Center (VDEC), the University of Tokyo, in collaboration with Cadence Design Systems, Inc. and Synopsis, Inc. The Josephson circuits were fabricated in the clean room for analog-digital superconductivity (CRAVITY) in National Institute of Advanced Industrial Science and Technology (AIST) with AIST 10 kA/cm² Nb high-speed standard process (HSTP). The CMOS circuits were fabricated in chip fabrication program of VDEC in collaboration with Rohm Corporation and Toppan Printing Corporation.

REFERENCES

- [1] D. Mamaluy and X. Gao, "The fundamental downscaling limit of field effect transistors," *Appl. Phys. Lett.*, vol. 106, no. 19, May 2015, Art. no. 193503.
- [2] K. K. Likharev and V. K. Semenov, "RSFQ logic/memory family: a new Josephson-junction technology for sub-terahertz-clock-frequency digital systems," *IEEE Trans. Appl. Supercond.*, vol. 1, no. 1, pp. 3–28, Mar. 1991.
- [3] Q. P. Herr, A. Y. Herr, O. T. Oberg, and A. G. Ioannidis, "Ultra-low-power superconductor logic," *J. Appl. Phys.*, vol. 109, no. 10, May 2011, Art. no. 103903.
- [4] O. A. Mukhanov, "Energy-efficient single flux quantum technology," *IEEE Trans. Appl. Supercond.*, vol. 21, no. 3 760–769, Jun. 2011.
- [5] M. Tanaka, M. Ito, A. Kitayama, T. Kouketsu and A. Fujimaki "18-GHz, 4.0-aJ/bit operation of ultra-low-energy rapid single-flux-quantum shift registers," *Jpn. J. Appl. Phys.*, vol. 51, no.5, May 2012, Art. no. 053102.
- [6] N. Takeuchi, D. Ozawa, Y. Yamanashi and N. Yoshikawa, "An adiabatic quantum flux parametron as an ultra-low-power logic device," *Supercond. Sci. Technol.* vol. 26, no. 3, Jun. 2013, Art. no. 035010.
- [7] K. Loe and E. Goto, "Analysis of flux input and output Josephson pair device," *IEEE Trans. Magn.*, vol. 21, no.2, pp. 884–887, Mar. 1985.
- [8] M. Hosoya, W. Hioe, J. Casas, R. Kamikawai, Y. Harada, Y. Wada, H. Nakane, R. Suda and E. Goto, "Quantum flux parametron: a single quantum flux device for Josephson supercomputer," *IEEE Trans. Appl. Supercond.*, vol. 1. no. 2, pp. 77-89, Jun. 1991.
- [9] K. Likharev, "Dynamics of some single flux quantum devices: I. Parametric qnantron," *IEEE Trans. Magn.*, vol. 13, no. 1, pp. 242–244, Jan. 1977.
- [10] J. G. Koller and W. C. Athas, "Adiabatic Switching, Low Energy Computing, And The Physics Of Storing And Erasing Information," *Workshop on Physics and Computation* (IEEE) pp 267–70, Oct. 1992.
- [11] N Takeuchi, Y Yamanashi, N Yoshikawa, "Energy efficiency of adiabatic superconductor logic," *Supercond. Sci. Technol.* vol. 28, no. 1, 2017, Art. no. 015003.
- [12] N. Takeuchi, T. Yamae T, C. Ayala, H. Suzuki, and N. Yoshikawa, "An adiabatic superconductor 8-bit adder with $24 k_B T$ energy dissipation per junction," *Appl. Phys. Lett.* vol. 114, no. 4, 2019, Art. no. 042602.
- [13] U. Ghoshal, H. Kroger, and T. Van Duzer, "Superconductor-semiconductor memories," *IEEE Trans. Appl. Supercond.*, vol. 3, pp. 2315-2318, March 1993.
- [14] Q. Liu, T. Van Duzer, X. Meng, S. R. Whiteley, K. Fujiwara, T. Tomida, K. Tokuda, and N. Yoshikawa, "Simulation and Measurements on a 64-kbit Hybrid Josephson-CMOS Memory," *IEEE Trans. Appl. Supercond.*, vol. 15, pp. 415-418, June 2005.
- [15] T. Van Duzer, L. Zheng, S. R. Whiteley, H. Kim, J. Kim, X. Meng and T. Ortlepp "64-kb Hybrid Josephson-CMOS 4 Kelvin RAM with 400 ps Access Time and 12 mW Read Power," *IEEE Trans. Appl. Supercond.*, vol. 23, no.3 p. 1700504, June 2013.
- [16] G. Konno, Y. Yamanashi and N. Yoshikawa, "Fully Functional Operation of Low-Power 64-kb Josephson-CMOS Hybrid Memories," *IEEE Trans. Appl. Supercond.*, vol. 27, no.4, Jun. 2017, Art. no. 1300607.
- [17] I. Kuon, R. Tessier, and J. Rose, "FPGA architecture: Survey and challenges," *Found. Trends Electron. Des. Autom.*, vol. 2, no. 2, pp. 135–253, Apr. 2008.
- [18] See for example: <https://www.xilinx.com/>
- [19] C. J. Fourie and H. van Heerden, "An RSFQ superconductive programmable gate array," *IEEE Trans. Appl. Supercond.*, vol. 17, no. 2, pp. 538–541, Jun. 2007.
- [20] N. K. Katam, O. A. Mukhanov and M. Pedram, "Superconducting Magnetic Field Programmable Gate Array," *IEEE Trans. Appl. Supercond.*, vol. 28 no. 2, Mar. 2018, Art. no. 1300212.
- [21] N. Takeuchi, S. Nagasawa, F. China, T. Ando, M. Hidaka, Y. Yamanashi, N. Yoshikawa, "Adiabatic quantum-flux-parametron cell library designed using a 10 kA cm⁻² niobium fabrication process," *Supercond. Sci. Technol.* vol. 30, 2017, Art. no. 035002.
- [22] N. Takeuchi, Y. Yamanashi, and N. Yoshikawa, "Adiabatic quantum-flux-parametron cell library adopting minimalist design," *J. Appl. Phys.*, vol. 117, no. 17, 2015, Art. no. 173912.
- [23] N. Tsuji, N. Takeuchi, C Ayala, Y. Yamanashi, and N. Yoshikawa, "Design and Implementation of a 16-Word by 1-Bit Register Files Using Adiabatic Quantum Flux Parametron Logic," *IEEE Trans. Appl. Supercond.*, vol. 27, no. 4, Jun. 2017, Art. no. 1300904.
- [24] S. K. Tolpygo, V. Bolkhovsky, T. Weir, A. Wynn, D. Oates, L. Johnson, and M. Gouker, "Advanced Fabrication Processes for Superconducting Very Large-Scale Integrated Circuits," *IEEE Trans. Appl. Supercond.*, vol. 26, no. 3, Apr. 2016, Art. no. 1100110.
- [25] T. Ando, S. Nagasawa, N. Takeuchi, N. Tsuji, F. China, M. Hidaka, Y. Yamanashi and N. Yoshikawa, "Three-dimensional adiabatic quantum-flux-parametron fabricated using a double-active-layered niobium process," *Supercond. Sci. Technol.* vol. 30, 2017, Art. no. 075003.